

# Solar Cycle Variation of Sustained Gamma Ray Emission from the Sun

Nat Gopalswamy<sup>1</sup>, Pertti Mäkelä<sup>1,2</sup>, Seiji Yashiro<sup>1,2</sup>, Sachiko Akiyama<sup>1,2</sup>, Hong Xie<sup>1,2</sup>, and  
G. Sindhuja<sup>1,2,3</sup>

<sup>1</sup>NASA Goddard Space Flight Center, Greenbelt, Maryland

<sup>2</sup>The Catholic University of America, Washington, DC

<sup>3</sup>Institute of Experimental and Applied Physics, Kiel University, Kiel, Germany

Submitted to: Solar Physics, November 28, 2025

## ABSTRACT

We investigated the occurrence rate of the sustained gamma ray emission (SGRE) events from the Sun using data obtained by the Large Area Telescope (LAT) on board the Fermi satellite since its launch in 2008. The data cover the whole of solar cycle (SC) 24 and the rising and maximum phases of SC 25. One of the challenges was to estimate the number of SGRE events in SC 25 because of a solar array drive assembly's malfunction starting in March 2018 that resulted in a large reduction in solar coverage by LAT. This is likely the reason for the small number (15) of SGRE events observed during the first 61 months of SC 25, whereas 25 events were observed during the weaker SC 24 over the corresponding epoch. Over the first 61 months, the average sunspot number (SSN) increased from 56.9 in SC 24 to 79.0 in SC 25. Other energetic events closely related to SGREs, viz., fast and wide (FW) coronal mass ejections (CMEs) and decameter-hectometric (DH) type II bursts also increased significantly in SC 25 by 29% and 33%, respectively when normalized to SSN. Therefore, the increase in solar activity should result in a higher number of SGREs in SC 25. We estimated the number of SGREs in SC 25 using three methods. (i) If the SGRE number varies commensurate FW CMEs and DH type II bursts, SC 25 should have 45-47 SGRE events ( $25 \times 1.29$  and  $25 \times 1.33$ ). (ii) In SC 24, ~17% of FW CMEs and 25% of DH type II bursts were associated with SGRE events. If the same association rate prevails in SC 25, we should have 46 SGRE events in this cycle. (iii) Since SGRE events are invariably associated with >100 keV hard X-ray (HXR) bursts, we identified DH type II bursts associated with >100 keV HXR bursts from Fermi's gamma ray burst monitor (GBM) during LAT data gaps. Based on our finding that SGRE events in SCs 24 and 25 were all associated with HXR bursts of duration  $>\sim 5$  min, we found only 27 of the 79 LAT-gap type II bursts had >100 keV HXR bursts with duration  $>\sim 5$  min. These DH type II bursts are likely to indicate SGRE, bringing the total number of SGRE events to 42 (15 observed + 27 inferred). Thus, the three methods provide similar estimates of the number of SGRE events in SC 25. We, therefore, conclude that SC 25 is stronger than SC 24 based on the estimated number SGRE events.

Other energetic phenomena such as halo CMEs, ground level enhancement (GLE) events, and intense geomagnetic storms are also consistent with a stronger SC 25.

## 1. Introduction

The level of solar activity is a key factor that decides the frequency and intensity of solar eruptions (flares and coronal mass ejections (CMEs)) and their space weather consequences. CMEs result in large solar energetic particle (SEP) events via the shock they drive and cause intense geomagnetic storms when CMEs directly impinge upon Earth's magnetic field. The level of solar activity is typically quantified using the sunspot number (SSN). High SSN indicates a high abundance of closed magnetic field regions, which are seats of solar eruptions. Therefore, one expects more energetic events such as ultrafast CMEs and major solar flares during solar maxima. During solar minima, eruptions are weak and occur only from quiescent filament regions. Energetic phenomena with severe space weather consequences show long-term variability in their occurrence rate somewhat similar to SSN: fast and wide (FW) CMEs, halo CMEs, large SEP events, intense geomagnetic storms, interplanetary type II radio bursts, coronal and interplanetary (IP) shocks, and IP CMEs (ICMEs). FW CMEs are defined as those with speed  $\geq 900 \text{ km s}^{-1}$  and width  $\geq 60^\circ$  (Gopalswamy et al. 2001). Large SEP events are those with proton intensity  $\geq 10 \text{ pfu}$  in the  $>10 \text{ MeV}$  GOES energy channel. An intense geomagnetic storm is characterized by the disturbance storm time (Dst) index  $\leq -100 \text{ nT}$ . Solar activity also modulates the physical conditions of the heliosphere. For example, the total pressure in the heliosphere is low during weak solar cycles affecting the physical properties of CMEs observed in the heliosphere (Gopalswamy et al. 2014; 2015a; 2023a). Two phenomena that show variations over and above that in SSN are ground level enhancement (GLE) in SEPs and intense geomagnetic storms.

Solar cycles 23 and 24 had the most complete observations of CMEs, considered to be key source of SEPs and geomagnetic storms. Solar cycle 24 has proved to be the weakest solar cycle in the *Space Age*. The weak activity of this cycle resulted in mild space weather: the number of large SEP events and intense geomagnetic storms decreased by 74% and 55%, respectively relative to SC 23. These decreases are significantly larger than the 39% reduction in SSN and 48% decrease in the number of FW CMEs (Gopalswamy et al. 2022). The number of GLE events showed extreme reduction: 16 in SC 23 vs. just 2 in SC 24 (i.e., by 87%). Thus, the highest energy particle events seem to be a very sensitive indicator of the cycle strength.

A phenomenon closely related to GLE events is the sustained gamma-ray emission (SGRE) from the Sun. SGRE was first recognized by Forrest et al. (1985) as emission lasting beyond the impulsive phase of the associated solar flare. Only a handful of SGRE events were recorded from the time of discovery in early 1980s until the advent of the Large Area Telescope (LAT, Atwood et al. 2009) on board the Fermi satellite (Thompson and Wilson-Hodge, 2022). A key characteristic of SGRE events is their association with the most energetic CME population,

similar to that causing GLEs (Gopalswamy et al. 2018). The connection is understandable because the underlying particles are accelerated by the same CME-driven shock. Thus, GLEs and SGRE are indicators of the highest energy particles accelerated by CME-driven shocks. In order to detect GLEs, the observer needs to be well-connected to the eruption region, so the high-energy particles can readily travel to the detector. This is the reason GLEs are generally detected from the western hemispheric eruptions, that too when the source is located close to the ecliptic (Gopalswamy et al. 2013; Gopalswamy and Mäkelä 2014; Gopalswamy et al. 2021). The lack of magnetic connectivity, therefore, is one of the main reasons for the rarity of GLE events. Fortunately, as electromagnetic radiation, SGRE is not affected by magnetic connectivity. This has been demonstrated by the occurrence of SGRE events from all across the solar disk, including from poorly connected east-limb regions (Share et al. 2018; Gopalswamy et al. 2019a; Ajello et al. 2021), and CMEs heading at large angles from the ecliptic. Therefore, SGRE events are better indicators of energetic eruptions that accelerate  $>300$  MeV protons.

Since SGREs are closely related to energetic CMEs from active regions, we expect them to occur in greater numbers in SC 25 because this cycle is stronger than SC 24 (e.g., Nandy 2021). However, a preliminary investigation showed that the number of SGRE events declined in SC 25 by  $\sim 40\%$ , while the sunspot number (SSN) increased by the same amount over the rise to maximum phases in each cycle (Gopalswamy et al. 2025a). The SGRE trend is also opposite to that of related phenomena such as decameter-hectometric (DH) type II radio bursts and FW CMEs. Gopalswamy et al. (2025a) concluded that  $\sim 3$  times more SGRE events are expected than the observed 15 events in SC 25. The reduction in the observed number of SGRE events seems to be due to a mechanical problem with the solar array drive assembly (SADA) that started on March 16, 2018. Because of this problem, SADA was not able to rotate the array for continuous illumination by the Sun. Following the SADA anomaly, the Sun is kept toward the edge of the LAT field of view (FOV) so that the array remains illuminated during orbit day. Such an arrangement reduced the Sun exposure resulting in large Fermi/LAT data gaps extending over a week at a time. The purpose of this paper is to estimate the number of SGRE events that might have occurred during these gaps and hence check the strength of SC 25 relative to SC 24.

In order to estimate the number of SGRE events that might have occurred during Fermi/LAT gaps, we shall make use of the close connection among hard X-ray (HXR) bursts, SEP events, and FW CMEs (Garcia 1994; Kiplinger 1995; Ling and Kahler 2020; Kahler and Ling 2020). We extend this connection to DH type II bursts. Share et al. (2018) reported that all SGRE events in SC 24 they studied were associated with an impulsive phase HXR burst at energies  $>100$  keV and suggested that such HXR emission is a necessary condition for SGRE. Flares with  $<100$  keV HXR bursts were not associated with SGRE, had lower soft X-ray power, slower CMEs, and weaker metric type II burst association; the HXR bursts also had steeper spectra. They examined a control sample of  $\sim 95$  events that met at least one of the following criteria: (i) presence of a fast CME (speed  $\geq 800$  km s $^{-1}$ ), (ii) association with SEP events with peak flux  $\geq 1$

pfu in the  $>10$  MeV integral channel, and (iii) involvement of HXR burst at energies  $>100$  keV. A subset of 19 events satisfied criteria (i) and (iii), out of which 14 (or 74%) were associated with SGRE. They could not rule out the presence of an SGRE in the remaining 5 events because they are all limb events (in which the observed gamma-ray flux is greatly reduced, see Gopalswamy et al. 2021) and the unfavorable Fermi/LAT duty cycle. They suggest that  $>100$  keV HXR emission may indicate flare-site acceleration of sub-MeV protons that serve as seed particles for further acceleration by the accompanying CME-driven shock. This close association between impulsive  $>100$  keV HXR bursts and SGRE is significant for our investigation. We shall make use of this Share criterion to estimate the number of SGRE events that might have occurred during Fermi/LAT data gaps.

## 2. Observational Results

SGRE events from SC 24 Fermi/LAT observations have been compiled and reported in a number of catalogs (Allafort et al. 2018; Share et al. 2018; Gopalswamy et al. 2019a; Ajello et al. 2021). For SC 25, we started with the SGRE candidates ([https://hesperia.gsfc.nasa.gov/fermi\\_solar/](https://hesperia.gsfc.nasa.gov/fermi_solar/)) compiled by the Fermi team. We confirmed these events using light curves and compiled related energetic phenomena. We also use Fermi's Gamma-ray Burst Monitor (GBM, Meegan et al. 2009) data from [http://hesperia.gsfc.nasa.gov/fermi/gbm/qlook/orbit\\_plots/](http://hesperia.gsfc.nasa.gov/fermi/gbm/qlook/orbit_plots/) in examining the hard X-ray flare activity during the study period. These data are particularly important for identifying flares during Fermi/LAT data gaps. Finally, we also use information from Konus-Wind (<https://www.ioffe.ru/LEA/kw/index.html>, Aptekar et al. 1995) to determine the onset times of some partially observed GBM HXR bursts. In doing so, we make use of the information available at the CDAW data center (<https://cdaw.gsfc.nasa.gov>): the CME catalog consisting of all CMEs manually identified ([https://cdaw.gsfc.nasa.gov/CME\\_list](https://cdaw.gsfc.nasa.gov/CME_list), Yashiro et al. 2004; Gopalswamy et al. 2009; Gopalswamy et al. 2024). We also use the halo CME catalog ([https://cdaw.gsfc.nasa.gov/CME\\_list/halo/halo.html](https://cdaw.gsfc.nasa.gov/CME_list/halo/halo.html), Gopalswamy et al. 2010), which provides additional information such as deprojected speed and CME source location on the Sun. These two catalogs are compiled primarily from images obtained by the Large Angle and Spectrometric Coronagraph (LASCO, Brueckner et al. 1995) on board the Solar and Heliospheric Observatory (SOHO) mission. Type II radio bursts in the DH wavelength are indicative of shocks in the corona and interplanetary (IP) medium driven by CMEs. These bursts as observed by the radio and plasma wave (WAVES) experiment on board the Wind (Bougeret et al. 1995) and the Solar Terrestrial Relations Observatory (STEREO, Bougeret et al. 2008) have been compiled and listed ([https://cdaw.gsfc.nasa.gov/CME\\_list/radio/waves\\_type2.html](https://cdaw.gsfc.nasa.gov/CME_list/radio/waves_type2.html), Gopalswamy et al. 2019b). This catalog features radio dynamic spectra showing type II bursts and the associated phenomena such as flares and CMEs. Large SEP events (proton intensity  $\geq 10$  pfu in the  $>10$  MeV energy channel) obtained from GOES proton data and the associated eruptive events are available at [https://cdaw.gsfc.nasa.gov/CME\\_list/sepe/](https://cdaw.gsfc.nasa.gov/CME_list/sepe/). The sunspot number (SSN) V2.0 is available at the Sunspot Index and Long-term Solar Observations (SILSO) web site located at

<https://wwwbis.sidc.be/silso/infosnmtot>, which we use to derive an average SSN over the first 61 months in SCs 24 and 25.

**Table 1.** Energetic events associated with SGRE in Solar Cycles 24 and 25

Property	SC 24 <sup>b</sup>	SC 25 <sup>b</sup>	SC25/SC24
Averaged SSN	56.9	79.0	1.39
# Halo CMEs	192 (3.37) <sup>a</sup>	247 (3.12)	1.29 (0.93)
# FW CMEs	149 (2.62)	268 (3.39)	1.80 (1.29)
# DH Type II bursts	99 (1.74)	183 (2.32)	1.85 (1.33)
# Intense magnetic storms	12 (0.21)	18 (0.23)	1.5 (1.06)
# $\geq$ M1.0 flares	389	1525	3.92 (2.82)
# $\geq$ 10 pfu SEP events	30 (0.53)	35 (0.44)	1.17 (0.83)
# GLE events	1 (0.02)	4 (0.05)	4.0 (2.50)
# DH Type II bursts	99 (1.74)	183 (2.32)	1.85 (1.33)
#SGRE events	25 (0.44)	15 (0.19)	0.60 (0.43)
#SGRE/#FW CMEs	0.17	0.05	0.31
#SGRE/#DH type II	0.25	0.08	0.30
#SGRE/#SEP events	0.83	0.40	0.48

<sup>a</sup>The numbers in parentheses are normalized to the corresponding SSN

<sup>b</sup>First 61 months of cycles 24 and 25 are compared.

## 2.1 Energetic Events in SCs 24 and 25

Table 1 compiles the number of energetic events (halo CMEs, FW CMEs, DH type II bursts, intense geomagnetic storms, major soft X-ray flares (flare class  $\geq$  M1.0), large SEP events, and GLE events. These numbers are compared between SCs 24 and 25 over the first 61 months in each cycle (2009 December 1 to 2013 December 31 in SC 24; 2019 December 1 to 31 December 2024 in SC 25). The monthly mean SSN are averaged over the first 61 months in each cycle and used as reference. Also listed are the number of SGRE events over the same epochs in the two cycles. We have compared the numbers directly and by normalizing them to SSN. Normalization accounts for the dependence of the number of events on solar activity. Table1 shows that the

average SSN in SC 25 is 79.0, increasing from 56.9 in SC 24 pointing to a stronger SC 25 by 39%.

When CMEs appear to surround the occulting disk of the observing coronagraph in sky-plane projection, they are called halo CMEs (Howard et al. 1982; 1985; Gopalswamy et al. 2010). Halo CMEs have been found to be a sensitive indicator of solar cycle strength in that weak cycles have a higher halo CME abundance (Gopalswamy et al. 2015b; 2023a). There are clearly more halo CMEs in SC 25 but when normalized to SSN, the halo CME abundance decreases by 7%. Thus, the lower halo abundance confirms that SC 25 is stronger than SC 24. Cumulative distributions of CME speeds (e.g., Gopalswamy 2018) indicates that FW CMEs are responsible for many of the heliospheric consequences of CMEs. In Table 1, the number of FW CMEs in SC 25 is 268, much larger than what was observed in SC 24 (149) over the same epoch. This corresponds to an 80% increase in SC 25. When normalized to SSN, the number of FW CMEs is still higher by ~29%. DH type II bursts are low-frequency radio bursts produced by electrons accelerated in CME-driven shocks. The underlying CMEs are known to be FW (Gopalswamy et al. 2001; 2019b). Not surprisingly, the number of DH type II bursts more than doubled in SC 25, reflecting the enhanced number of FW CMEs in the cycle. When normalized to SSN, the increase in the number of DH type II bursts in SC 25 by ~33% similar to the increase observed in the number of FW CMEs. These increases are over and above that in SSN potentially indicating some non-spot eruptions. Interestingly, the ratio of the number of DH type II bursts to that of FW CMEs remains the same in the two cycles (66% in SC 24 and 68% in SC 25) again indicating a close physical relationship between the two phenomena.

One of the consequences of FW CMEs heading toward Earth is geomagnetic storms. The number of intense geomagnetic storms ( $Dst \leq -100$  nT) in SC 25 is 18 compared to 12 in SC 24 during the first 61 months in each cycle. The increase also holds when normalized to SSN by 6%. The number of large SEP events increased only slightly in SC 25 but when normalized to SSN, it shows a slight (~13%) decline. The number of GLE events quadrupled in SC 25 and the normalized number shows an increase of 150%. The detection of SEP events and GLE events is affected by their magnetic connection to the observer (GOES and ground based neutron monitors). The other aspect of solar eruptions, viz., major soft X-ray flares with intensity  $\geq M1.0$  also points to a stronger SC 25: the number of major flares quadrupled relative to SC 24. When normalized to SSN, the number of major flares is still higher by ~182%. While most of the numbers in Table 1 definitely indicate a stronger SC 25, the number of SGRE events shows a significant (~40%) decline from 25 in SC 24 to just 15 in SC 25; the decline is similar (~43%) when normalized to SSN. We expect the number of SGREs to roughly follow the solar cycle variation of the number of FW CMEs and DH type II bursts. The number of SGRE events normalized to the number of DH type II bursts (FW CMEs) is 0.25 (0.17) in SC 24, whereas it drops to 0.08 (0.05) in SC 25. The drop is most likely due to the reduction in LAT's Sun exposure due to the SADA problem.

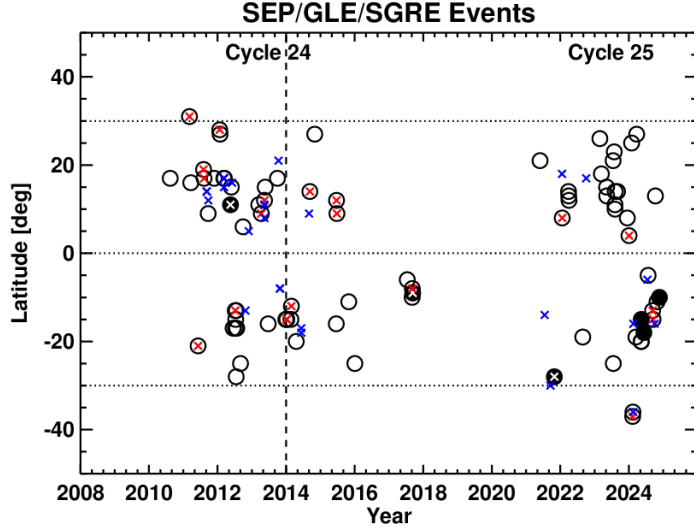


Figure 1. Time-latitude plot of the solar sources of large SEP events and SGRE events in solar cycles 24 and 25. SEP events are marked by black circles. Filled circles represent ground level enhancement (GLE) events in SEPs. SEP events with SGRE are shown by red x symbols within the black circles. GLEs with SGRE are marked with white x. The blue x symbols denote SGRE events not associated with SEPs. The data points to the left of the vertical dashed line denote events from the first 61 months (December 2009 to December 2013) of cycle 24 and are compared with the corresponding epoch in cycle 25 (December 2019 to December 2024). There are 45 events in SC 24 (30 SEP events with only 10 having SGRE association; 15 SGRE events occurred with no large SEP events detected by GOES). There are 43 events plotted in SC 25 (29 SEP events with only 6 associated with SGRE; 8 SGRE events occurred with no large SEP events).

## 2.2 Relative Variation of CME Source Latitudes associated with SGRE and SEP Events

Even though SEP events are closest to SGRE events (they share the same acceleration source under the shock paradigm), the latter often occur without the former because of the magnetic connectivity requirement. Some SEP events occur when the particle background is high due to a preceding eruption and hence may not be identified as a separate event. The fact that a large number of SGRE events occur without SEP association is illustrated in Fig. 1, which shows the source locations of large SEP and SGRE events as a function of time. There are 15 SGRE events in SC 24 and 8 in SC 25 with no  $\geq 10$  pfu SEP event detected by GOES; however, almost all these SGRE events are associated with FW CMEs and DH type II bursts. We see that only 6 of the 35 SEP events (or 17%) have SGRE association in SC 25 as opposed to 10 of the 30 SEP events or (33%) in SC 24. The SEP events include one GLE event in SC 24 and 4 in SC 25. The second GLE event in SC 24 occurred close to the end of the cycle, therefore, is not within the first 61 months. Among the four GLEs in SC 25, only the first one on 2021 October 28 was

associated with SGRE. The second GLE on 2024 May 11 occurred during a Fermi/LAT data gap. The third GLE occurred on 2024 June 8, the only front-side GLE not associated with SGRE. This needs further investigation because all the related phenomena such as large SEP event extending to energies  $>100$  MeV and intense long-duration DH type II burst. Finally, the last GLE on 2024 November 21 occurred  $\sim 20^\circ$  behind the west limb and was not associated with SGRE. Figure 1 also makes it clear that the SEP events and SGRE events all occur in the active region belt ( $\pm 30^\circ$  in latitudes) where high magnetic energy is generally available to power these energetic events.

It must be noted that all the events plotted in Fig. 1 are associated with DH type II bursts. Given the moderate association between SEP and SGRE events, DH type II bursts can be seen as better indicators of SGRE events. In order to understand the impact of Fermi/LAT data gaps on the SGRE event count in SC 25, we first identify the data gaps, identify the high-energy events during the gaps, and then estimate the number of SGRE events in the cycle. Such an estimate will tell whether the SGRE events are consistent with the fact that SC 25 is slightly stronger than SC 24 as indicated by other energetic events. As a proxy for high energy events, we take DH type II bursts because they are closest to SGRE and a subset of FW CMEs.

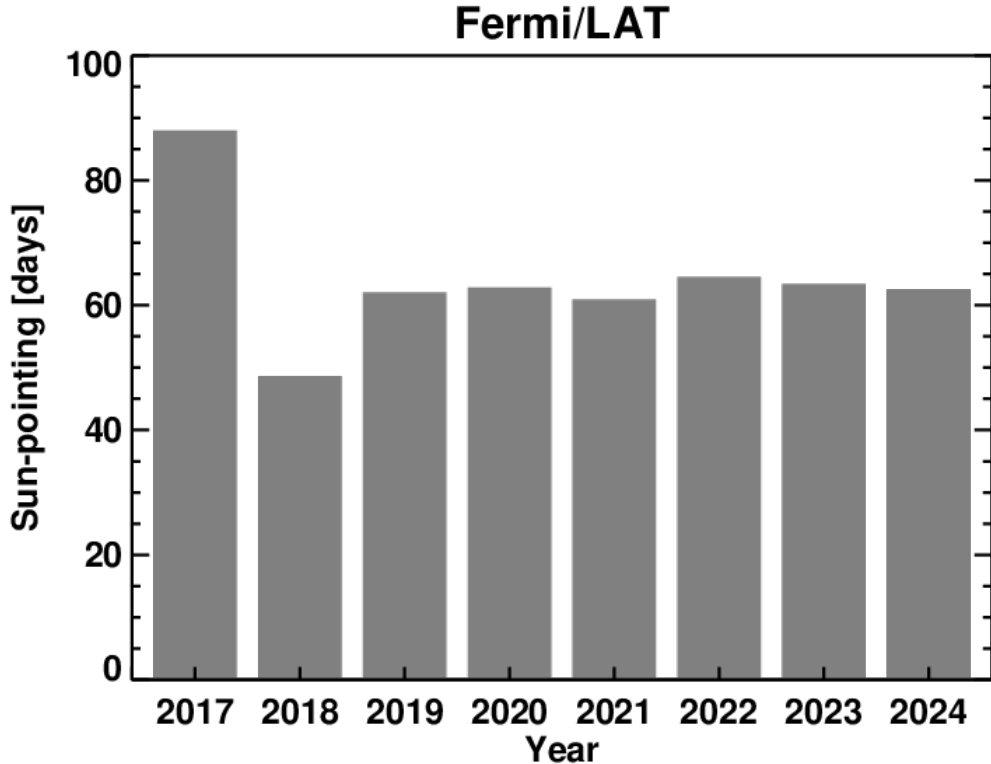


**Figure 2.** Effective solar exposure (number of days) during each year since 2017. The exposure reduction is by about one third after the SADA anomaly that started in March 2018. One can expect a one-third reduction in the number of SGRE events in solar cycle 25 if we assume that the SGRE occurred with the same rate as in SC 24.

### 2.3 Fermi/LAT Data Coverage in SC 25

The reduced solar coverage started on 2018 March 16, towards the end of SC 24. The drive of one of the two solar arrays of the Fermi satellite experienced an anomaly that led to the reduction ([https://fermi.gsfc.nasa.gov/ssc/observations/types/post\\_anomaly/](https://fermi.gsfc.nasa.gov/ssc/observations/types/post_anomaly/)). Although the solar array in question is fully functional, it got stuck at an angle to the LAT boresight because SADA was not able to rotate the array. In order for the non-rotating array to be illuminated, the Sun is kept toward the edge of the LAT FOV resulting in the observational gaps (1-3 weeks at a time) in the Sun exposure. The maximum LAT effective area is reduced to below 4000 cm<sup>2</sup> in 2019 and later years compared to a maximum of 5500 cm<sup>2</sup> in the pre-2018 period.

Figure 2 shows Fermi/LAT's annual Sun exposure as an effective number of days. The anomaly years (2018 onwards) are compared with one pre-anomaly year (2017). The total annual exposure time during the pre-anomaly years is ~90 days per year determined by the satellite orbital period (~95 min) and the amount of time (~20-30 min per orbit) LAT was pointed to the Sun. The anomaly year 2018 had a larger reduction while redesigning the observing modes (the total annual Sun exposure was only ~50 days). In the years after 2018, the Sun exposure was between 60 and 65 days, which corresponds to a reduction of ~ 30%. Lack of LAT observations is substantial, so any SGRE event occurring during these gaps will not be counted. One can infer that more SGRE events might have occurred during the LAT gaps simply based on the fact that there were many FW CMEs, large SEP events, and DH type II radio bursts – the key phenomena associated with SGREs – occurred during the gaps.

Table 2. Fermi/LAT data gaps and the number of energetic events

Year	#SGRE	#Gap days	#FW CMEs	#DH Type II	#SEP
2018	0	132.5	0 (0)	0 (0)	0 (0)
2019	0	137.0	0 (0)	1 (0)	0 (0)
2020	0	119.5	2 (0)	2 (0)	0 (0)
2021	2	130.5	11 (1)	15 (4)	2 (0)
2022	4	133.0	61 (19)	34 (8)	5 (0)
2023	1	133.5	86 (30)	55 (28)	12 (7)
2024	8	133.0	108 (35)	77 (39)	16 (6)

Table 2 shows the observed number of SGRE events in SC 25 (column 2) along with the number of Fermi/LAT data gaps in each year (column 3), fast ad wide CMEs, DH type II bursts, and large SEP events. The numbers in parentheses correspond to events occurring during Fermi/LAT data gaps. We see substantial numbers of energetic events occurring during the gaps, especially during the solar maximum years (2022-2024). In SC 24, the number of FW CMEs and DH type II bursts is 149 and 99, respectively. The corresponding numbers in SC 25 are 268 and 183 (see Table 1). If the fraction of FW CMEs (17%) and DH type II bursts (25%) remains

similar in SC 25, we expect  $\sim$ 45 and 47 SGRE events, respectively. This would imply that 30-32 SGRE events should have occurred during the LAT gaps.

Let us consider the 79 DH type II bursts that occurred during the gaps (Table 2). Recall that only a quarter of the DH type II bursts are typically associated with SGRE (see Table 1). We need to determine which DH type II bursts are likely to be associated with SGRE events. For this purpose, we make use of the Share criterion (Share et al, 2018) that presence of  $>100$  keV hard X-ray bursts is necessary for the occurrence of an SGRE event. Fortunately, Fermi/GBM was observing the Sun more or less continuously, so we know how many  $>100$  keV HXR bursts occurred during LAT data gaps. If a DH type II burst is associated with a  $>100$  keV HXR burst, it is a good indicator of an SGRE event. Share et al. (2018) work was on SC 24 SGRE events. Here we confirm the  $>100$  keV HXR burst association in SC 25 SGRE events.

### 3. SGRE Events and Hard X-ray Bursts

In characterizing the association of HXR bursts with SGRE events, we consider the flux in the Fermi/GBM channel 100-300 keV, which we refer to as a  $>100$  keV event throughout the paper. While examining the  $>100$  keV HXR bursts during LAT gaps in SC 25, we found that most of the bursts were of short duration, typically less than a couple of minutes. Some bursts have durations of longer than  $\sim$ 5 minutes. Figure 3 shows two GBM HXR bursts identified during two different LAT data gaps. The HXR burst on 2024 October 9 corresponds to an X1.8 GOES flare from the disk center (N13W08) with start, peak, and end times of 01:25 UT, 01:56 UT, and 02:43 UT, respectively. The 100-300 keV count rate gets above the threshold (100 counts/s) around 01:41:37 UT, attains peak ( $\sim$ 3252 counts/s) at 01:47:10, and drops below the threshold level at 02:06:04 UT yielding a long duration (LD) of  $\sim$ 24.5 min. The background HXR is the difference between three most sunward detectors and three least sunward detectors. The background level is highly variable, so we chose the 100 counts/s as the threshold level to compute the duration. In some cases, the real background is much lower, so the use of the 100 counts/s threshold underestimates the duration (see later). The HXR burst on 2024 December 21 originates in an impulsive M1.9 GOES flare from S15E62. The SXR flare has a short duration,  $\sim$ 9 min with start, peak, and end times of 00:33 UT, 00:38 UT, and 00:42 UT, respectively. The short duration (SD) HXR burst goes above the 100 counts/s level only for 64 s with its peak (2046 counts/s) coinciding with the SXR peak. The LD burst was associated with a fast ( $1435 \text{ km s}^{-1}$ ) double-whammy halo CME: it produced a large SEP event with the  $>10$  MeV proton intensity exceeding 1000 pfu and a super-intense geomagnetic storm ( $\text{Dst} \sim -333 \text{ nT}$ ). The deprojected speed is  $\sim 1857 \text{ km s}^{-1}$ . The  $>100$  MeV SEP intensity remained high for more than a day, suggesting that the SEP event is likely to have produced an SGRE event that was not observed due to the LAT gap.

The SD burst was also associated with a narrow ( $\sim 40^\circ$ ) and slow CME associated with a surge observed by STEREO's Extreme UltraViolet Imager (EUVI, Howard et al. 2008) at  $304 \text{ \AA}$  (00:45 – 00:55 UT). This CME occurred when the SEP background was high due to a previous

CME elevated, but SEPs are not expected from such weak and narrow CMEs. The LD event had an intense DH type II burst that lasts at least until 10 UT the next day. The LD HXR burst was associated with a DH type III burst that lasted for  $\sim$ 30 min. The SD HXR was associated with a very short-lived ( $\sim$ 1 min) type III burst, but no type II burst. Thus, in all respects, the LD HXR burst is likely to be associated with an SGRE, while it is unlikely that the SD HXR has such an association.

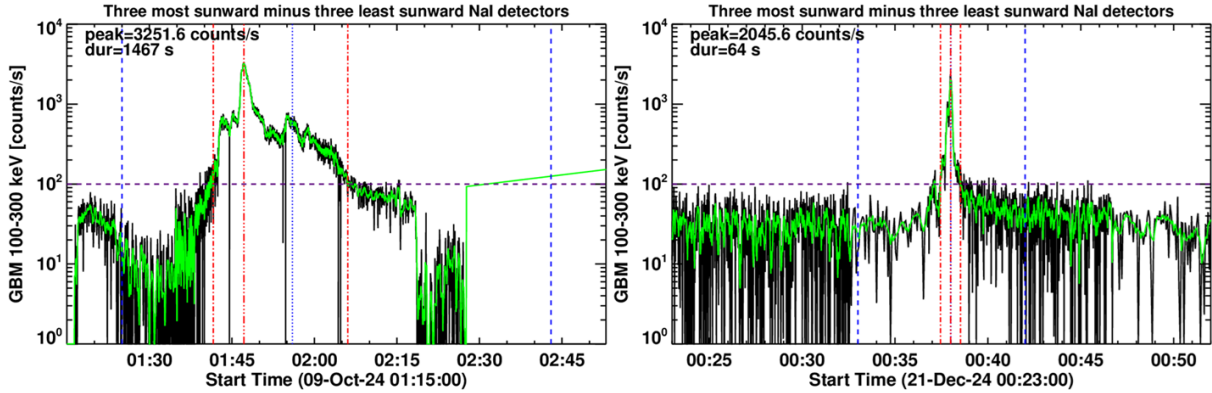


**Figure 3.** Plots of GBM count rates of two  $>100$  keV hard X-ray bursts (left: 2024 October 9 around 01:15 UT and right: 2024 December 21 around 00:35 UT) in the 100-300 keV energy channel. The bursts occurred during LAT data gaps of 2024 October 8-21 and 2024 December 16-22. The black and green curves are the actual and 12 s averaged count rates. The three vertical red dot-dashed lines in each panel correspond to the onset, peak and end of the HXR burst. The horizontal dashed line at 100 counts/s represents the threshold level we used in identifying HXR bursts. The 100-300 keV HXR durations above 100 counts/s and the peak count rate are noted on the plots. The vertical blue dashed lines mark the start and end of the GOES soft X-ray flare with the vertical blue dotted line showing the GOES SXR peak time.

### 3.1 HXR Bursts Associated with SC 25 SGRE Events

In order to check if SC 25 SGRE events are associated with LD HXR bursts, we examined the  $>100$  keV Fermi/GBM data corresponding to the LAT events. We specifically use the 100-300 keV channel data to determine the duration and peak flux. The data were obtained with different time resolutions, but we smooth the data over 12 s. When GBM data are interrupted by Fermi night or SAA passage, we use Konus data when available in estimating the duration. We examined both the trigger mode and waiting mode data (Lysenko et al. 2022) to determine the HXR duration. We use the Konus G2 energy channel ( $\sim$ 80–300 keV), which is very similar to the GBM 100-300 keV channel. The Wind spacecraft is located at Sun-Earth L1, so the HXR background is very low and there is no satellite night unlike Fermi. We take the starting (ending) time as the earlier (later) of the GBM or Konus observations. The light travel time is  $\sim$ 5 s from L1 to Earth, so we corrected the Konus time for this. Table 3 shows the 15 SC 25 Fermi/LAT

SGRE events with the associated HXR bursts. Columns 1-5 give the date, HXR start and end times, duration above 100 counts/s, and the 100-300 keV peak count rate. Columns 6, 7, and 8 list the GOES SXR flare location, class and start time, respectively. The last two columns give the CME sky-plane speed and width (halo - H or partial halo - PH). The HXR start end times have a suffix letter G (Fermi/GBM) or K (Wind/Konus) to denote which instrument measured the time. Of the 15 SGRE events, only 10 have GBM and/or Konus data as listed in Table 2. The circumstances of the remaining 5 events are as follows. (i) The first SC 25 SGRE event on 2021 July 17 occurred during a Fermi/GBM data gap between July 16 and July 20. Besides, this event occurred  $\sim 50^\circ$  behind the east limb, so it is unlikely that a HXR emission would be detected by GBM or Konus. However, the event was associated with a HXR burst observed by the Spectrometer/Telescope for Imaging X-rays (STIX, Krucker et al. 2020) on board Solar Orbiter as reported by Pesce-Rollins et al. (2022). (ii) The 2022 January 18 SGRE had a GBM data gap, and no event was reported by Konus. (iii) The 2024 February 14 event was completely backsided with no HXR detector operating on the backside during the event. (iv) the 2024 September 9 event was also associated with a backside eruption but a HXR burst was detected by Solar Orbiter (Gopalswamy et al. 2025b). (v) The 2024 October 1 event occurred during Fermi night, but the onset, peak and early declining phases were observed by Konus, indicating that the HXR burst had a duration of at least  $\sim 4.2$  min. From the ten events with known start and end times of  $>100$  keV HXR bursts, we see that the durations are in the range 6 – 41.37 min with an average (median) value of 17.88 (14.11) min. Thus, the HXR durations in SGRE events are similar to those of the LD events found during LAT gaps (see Fig. 3 for an example). The association of  $>100$  keV HXR during SGRE events reported by Share et al. (2018) are confirmed with the additional constraint that the HXR duration is  $>5$  min. Of the 14 events with known GOES flare size, only three (or 21%) were of M-class, while all the remaining were of X-class. The CMEs are mostly halos with 5 (or 33%) partial halos.

**Table 2.** List of  $>100$  keV bursts and their duration during SC 25 SGRE events

DATE	Start UT <sup>a</sup>	End UT <sup>a</sup>	Dur [min]	Peak Count/s	Flare Location	Flare Class	Flare UT	CME V [km s <sup>-1</sup> ]	CME Width
2021/07/17	DG	DG	DG	DG	S20E140	M5.0	04:50	1228	H
2021/09/17	04:14:00G	04:20:00G	6.0	450	S30E100	X1.9 <sup>b</sup>	----	1370	PH
2021/10/28	15:27:30K	16:08:52G	41.37	2514	S28W01	X1.0	15:17	1519	H
2022/01/18	DG	DG	DG	DG	N18W54	M1.5	17:01	1014	PH
2022/01/20	05:54:07G	06:04:43G	10.60	2161	N08W68	M5.5	05:41	1431	PH
2022/10/02	20:20:13G	20:30:25G	10.22	9117	N18W50	X1.0	19:53	1086	H
2023/12/31	21:38:44K	22:08:26G	29.70	2566	N04E73	X5.0	21:36	2852	H
2024/02/09	13:01:44K	13:13:04K	11.33	5632	S37W98	X3.3	12:53	2782	H
2024/02/14	DG	DG	DG	DG	S36W160	???	03:55 <sup>c</sup>	2191	H
2024/02/16	06:50:55K	06:59:20G	8.42	12909	S19W86	X2.5	06:42	617	PH
2024/07/16	13:18:55K	13:35:48G	16.88	106	S06W85	X1.9	13:11	580	PH
2024/09/09	DG	DG	DG	DG	S13E131	X3.0 <sup>d</sup>	04:56	1522	H
2024/09/14	15:17:02G	15:36:15G	19.22	31516	S15E56	X4.5	15:13	2366	H
2024/10/01	DG	DG	DG	DG	S16E17	X7.1	21:58	598	H

2024/10/24	03:38:36G	04:03:37G	25.02	8099	S05E86	X3.3	03:30	2385	H
------------	-----------	-----------	-------	------	--------	------	-------	------	---

<sup>a</sup>G and K indicate that the time was determined from GBM and Konus data, respectively.

<sup>b</sup>Flare class reported in Pesce-Rollins et al. (2022) and Yashiro et al. (2024) based on EUV data

<sup>c</sup>Based on DH Type III burst onset

<sup>d</sup>From Gopalswamy et al. (2025b)

### 3.2 HXR Bursts Associated with SC 24 SGRE Events

Fermi/LAT observations during most of SC 24 had no major interruptions indicating normal solar coverage until March 16, 2018. The remaining time in SC 24 after the SADA anomaly was towards the end of the cycle, so there was no significant SGRE activity. The SGRE events observed in SC 24 provide a reference to compare those in SC 25 that had reduced solar coverage. Table 3 shows Fermi/GBM HXR bursts associated with SC 24 SGREs along with their durations and peak fluxes (see also Share et al. 2018). For 4 SGRE events, GBM had partial data gaps, so the peak HXR count rate is not available. In these cases, Konus observed the bursts fully, which we use in the table. We converted the Konus peak count rate K in the 80-300 keV channel to an equivalent GBM count rate G by establishing a correlation between the fluxes using 14 events in Table 3 observed by both instruments. The regression equation is  $G = 2.36K + 929.7$  with a correlation coefficient (cc) of 0.97. The Pearson's critical cc for 14 events is 0.780 with a chance coincidence probability  $p = 5 \times 10^{-4}$ .

**Table 3.** List of  $>100$  keV bursts and their duration during SC 24 SGRE events

DATE	Start UT <sup>a</sup>	End UT <sup>a</sup>	Dur [min]	Peak Count/s	Flare Location	Flare Class	Flare UT	CME V [km s <sup>-1</sup> ]	CME Width
2011/03/07	20:02:12G	20:42:00G	39.80	2120	N30W48	M3.7	19:43	2125	H
2011/06/02	DG	DG	DG	DG	S19E25	C3.7	07:22	976	H
2011/06/07	06:24:13G	06:42:01G	17.80	1453	S21W54	M2.5	06:16	1255	H
2011/08/04	03:48:59G	04:00:59G	12.00	2271	N19W36	M9.3	03:41	1315	H
2011/08/09	08:01:14G	08:08:14G	7.00	113214	N17W69	X6.9	07:48	1610	H
2011/09/06	22:17:50G	22:27:02G	5.60	59017	N14W18	X2.1	22:12	575	H
2011/09/07	22:35:27G	22:41:27G	6.00	19018	N14W28	X1.8	22:32	792	PH
2011/09/24	09:35:00G	09:44:24G	9.40	40038	N12E60	X1.9	09:21	1936	PH
2012/01/23	03:52:46G	04:11:00G	18.23	1444	N28W21	M8.7	03:38	2175	H
2012/01/27	18:09:51G	18:44:00G	34.15	550	N27W78	X1.7	17:37	2508	H
2012/03/05	03:55:39G	04:56:00G	60.35	1659	N17E52	X1.1	03:17	1531	H
2012/03/07	00:30:09G	01:28:08G	57.98	38009	N15E26	X1.3	01:05 <sup>c</sup>	1825	H
2012/03/09	03:37:50G	04:03:52G	26.03	363	N15W03	M6.3	03:22	950	H
2012/03/10	17:40:50G	18:05:36G	24.77 <sup>d</sup>	300 <sup>d</sup>	N18W26	M8.4	17:10	1296	H
2012/05/17 <sup>e</sup>	DG	DG	DG	DG	N11W76	M5.1	01:25	1582	H
2012/06/03	17:53:01G	17:55:01G	2.00	3313	N16E38	M3.3	17:48	605	PH
2012/07/06	23:00:25G	23:08:10K	7.75	125584 <sup>g</sup>	S17W52	X1.1	23:01	1828	H
2012/10/23	03:14:47G	03:19:47G	5.00	43856	S13E60	X1.8	03:13	243	NH
2012/11/27	15:55:25G	15:58:01G	2.60	1081	N05W73	M1.6	15:52	----	--

2013/04/11	07:08:25G	07:15:48G	7.38	424	N09E12	M6.5	06:55	861	H
2013/05/13	02:03:13G	02:10:14G	7.02 <sup>f</sup>	3000	N11E89	X1.1	01:53	1270	H
2013/05/13	16:04:13G	16:13:00G	8.78	45142	N11E85	X2.8	15:48	1850	H
2013/05/14	01:02:37G	01:23:01G	20.40	11346	N08E77	X3.2	00:00	2625	H
2013/05/15	01:36:39G	01:54:16G	17.62	1936	N12E64	X1.2	01:25	1366	H
2013/10/11	No HXR	No HXR	No HXR	No HXR	N21E103	M1.5 <sup>b</sup>	07:01	1200	H
2013/10/25	07:57:23K	08:19:00G	21.78	27072 <sup>g</sup>	S08E71	X1.7	07:53	587	H
2013/10/25	14:56:00G	15:15:00G	19.0	8400 <sup>g</sup>	S06E69	X2.1	14:51	1081	H
2013/10/28	14:02:01K	14:10:00G	6.0	21054 <sup>g</sup>	N06W75	M2.8	14:00	1073	NH
2014/02/25	00:42:21G	01:04:22G	22.02	192537	S12E82	X4.9	00:39	2147	H
2014/09/01	11:04:25G	11:29:48G	25.38	563	N14E127	X2.4 <sup>b</sup>	11:05	1901	H
2015/06/21	02:09:49G	02:20:00G	10.18	150	N13E16	M2.6	02:03	1366	H
2015/06/25	08:12:24G	08:29:24G	17.00	30910	N09W42	M7.9	08:02	1627	H
2017/09/06	11:55:29K	12:40:46G	45.28	113727	S08W33	X9.3	11:53	1571	H
2017/09/10	15:50:11G	16:39:47G	49.60	125484	S09W96	X8.2	15:35	3163	H

<sup>a</sup>G and K indicate that the time was determined from GBM and Konus data, respectively.

<sup>b</sup>Flare class of the behind-the-limb events is based on EUV data

<sup>c</sup>The preceding faster (2684 km s<sup>-1</sup>) CME at 00:24 UT accompanied by an X5.4 flare from the same active region is also associated with a >100 keV HXR burst that started during the spacecraft night; the duration of the day-time portion is ~30 min (00:30 to 01:00 UT). Konus data indicates an onset of 00:06:17 UT. The second HXR burst started before the first one ended. Both these eruptions were associated with a single >100 MeV LAT SGRE event.

<sup>d</sup>Duration and peak count rate are lower limits because the start and peak times are unknown.

<sup>e</sup>GLE event

<sup>f</sup>Lower limit because the spacecraft night started before the burst end

<sup>g</sup>Based on peak count rate from Konus modified using the correlation between peak count rates of SC 24 events observed by both Konus and GBM.

Twenty eight of the 34 events listed in Table 3 occurred during the first 61 months of SC 24. All SGRE events in SC 24 have associated >100 keV HXR bursts, except for three events: 2011 June 2, 2013 October 11, and 2012 May 17. The 2013 October 11 event occurred ~13° behind the limb, so it is possible that flare electrons were not able to precipitate on the front side to emit >100 keV HXR. The 2011 June 2 SGRE event had a GBM data gap and occurred under special circumstances of interacting CMEs (to be discussed later). We see that the HXR durations are in the range 2 – 60.35 min, similar to that in SC 25. Considering the 25 events with HXR data during the first 61 months, the mean and median durations are 17.78 min and 12.00 min. If we consider all the events in SC 24, the mean and median durations are not very different: 19.8 min and 17.62 min. The flares involved are also major, most of them being X-class with 13 out of 28 (or 46%) being of M-class. Most of the CMEs are halos or partial halos as in SC 25.

### 3.3 HXR Bursts Associated with DH Type II Bursts in LAT Gaps

In this subsection we consider all the DH type II bursts observed during LAT data gaps and their association with  $>100$  keV HXR bursts from Fermi/GBM and Wind/Konus. We do know that almost all SGRE events are associated with type II radio bursts, while only  $\sim 25\%$  of DH type II bursts are associated with SGRE events (see Table 1). Examining the association of  $>100$  keV HXR bursts we find that out of the 79 DH type II bursts that occurred during the LAT gaps, only 27 (or 34%) had associated HXR bursts. Out of the remaining 52 DH type II bursts, 26 had no HXR burst association. The remaining 26 DH type II bursts occurred during Fermi night or during South Atlantic Anomaly (SAA) crossing. Table 4 lists the 27 type II bursts with overlapping Fermi/GBM observations. A vast majority of the HXR bursts have long durations except for three events lasting for 0.77, 2.02, and 2.22 min. These durations are likely underestimates as will be discussed later in this subsection. Most of the flares in Table 4 are of X class, with 12 of them of M-class (or 44%), similar to what was observed during SGREs of SC 24. As in Tables 2 and 3, most of the CMEs are halos (19 out of 27 or 70%) with 5 partial halos (19%) and three non-halos (NH, 11%); the non-halos are normal CMEs with width  $<120^\circ$ . Having a large fraction of halos indicates that the CME population underlying DH type II bursts is very energetic (Gopalswamy et al. 2019b).

**Table 4.** List of  $>100$  keV HXR Bursts associated with DH type II bursts in LAT Data Gaps

DATE	STIME	ETIME	Dur [min]	HXR Flux	Flare Location	Class	Flare Time	CME V [km s $^{-1}$ ]	CME Width
2022/04/29	07:20:39K	07:21:25K	0.77	260	N25W37	M1.2	07:15	1292	PH
2023/02/17	19:57:39K	20:24:59G	27.33	1528	N25E64	X2.2	19:38	1315	H
2023/05/09	18:28:26K	18:56:23G	27.95	193	N13W31	M4.2	18:20	1209	H
2023/06/20	16:57:49G	17:08:59K	11.17	267	S17E73	X1.1	16:42	1113	H
2023/07/28	15:43:42K	16:11:50G	28.13	164	N23W94	M4.1	15:39	1896	H
2023/08/05	22:00:59K	22:21:01G	20.03	1058	N11W77	X1.6	21:45	1647	H
2023/08/07	20:37:35K	21:08:09K	30.57	244	N13W98	X1.5	20:30	1851	H
2023/09/19	09:32:44K	09:37:26K	4.70	115	N07E51	M1.8	09:23	418	PH
2023/09/19	20:08:38G	20:10:39G	2.02	1107	N08E45	M4.0	20:01	483	NH
2023/11/28	19:37:03G	19:50:51G	13.80	536	S16W00	M9.8	19:35	741	H
2024/05/03	02:18:24G	02:24:36G	6.20	3123	N25E07	X1.6	02:11	808	H
2024/05/08	04:46:52G	05:09:28G	22.60	116	S22W11	X1.0	04:37	530	H
2024/05/08	11:58:00K	12:12:58K	14.97	211	S20W17	M8.7	11:26	677	H
2024/05/09	08:59:39K	09:45:50G	46.18	308	S20W26	X2.2	08:45	1280	H
2024/05/09	17:30:37G	17:35:25G	4.80	363	S14W28	X1.1	17:23	1024	H
2024/05/10	06:42:02G	06:51:39G	9.62	12078	S17W34	X3.9	06:27	953	H
2024/05/11	01:14:24G	01:37:49G	23.42	56565	S15W45	X5.8	01:10	1614	H
2024/05/14	02:04:24G	02:10:36G	6.20	13609	S19W88	X1.7	02:03	881	NH
2024/05/14	16:46:24G	16:50:57K	4.55	146483	S18W96	X8.7	16:46	2010	H
2024/05/15	08:15:47G	08:37:55G	22.13	46539	S18W98	X3.5	08:13	1648	H
2024/07/28	10:35:39G	10:46:26G	10.78	129	S11W40	M7.7	10:27	918	NH
2024/08/02	04:38:26K	04:43:15K	4.82	167	S14W90	M7.3	04:23	1141	PH
2024/08/05	05:20:04K	05:24:50G	4.77	2097	S11E62	M6.1	05:36	973	PH

2024/08/07	13:46:11G	13:48:24G	2.22	1842	S11E03	M4.5	13:30	658	H
2024/09/22	21:22:38G	21:32:00K	9.37	141	S20E63	M3.7	21:12	1256	H
2024/10/09	01:42:27K	02:18:26G	35.98	3151	N13W08	X1.8	01:25	1435	H
2024/10/09	15:44:01G	15:48:25G	4.40	46286	S10W83	X1.4	15:44	874	PH

### 3.4 Comparing HXR properties during SGREs and DH Type II bursts

We have measured the HXR durations of SGREs (during SCs 24 and 25) and DH type II bursts that occurred during LAT data gaps in SC 25. From Tables 2-4, we see that the underlying CMEs are energetic, associated with major flares (M and X class), and the HXR bursts have long durations. The average sky-plane speeds are: 1549 km s<sup>-1</sup> (SC 24), 1699 km s<sup>-1</sup> (SC 25), and 1141 km s<sup>-1</sup> (DH type II). SGREs of SC 24 and DH type II bursts have similar fraction of M-class flares, while SC 25 SGREs have mostly X-class flares. Note that the sample size is small for SGREs in SC 25. Figure 4 (a-c) compare the >100 keV HXR duration distributions among (i) SGRE events in SC 24, (ii) SGRE events in SC 25, and (iii) LAT-gap DH type II bursts. The duration distributions are similar. The median HXR duration for 24 SGREs, SC 25 SGREs, and LAT-gap DH type II bursts are 12.0 min, 13.83 min, and 10.78 min, respectively. The median HXR duration is larger (17.62 min) when the full set of SC 24 SGREs. The mean durations are also similar: 17.78 min (SC 24) 17.88 (SC 25) and 14.8 min (LAT-gap DH type II bursts). Kolmogorov-Smirnov (KS) tests (Kirkman, 1996) comparing these durations taken two at a time show that these duration distributions are not statistically different. Table 3 shows these comparisons along with the KS test statistic D, which is the maximum difference between the cumulative distributions of a pair compared. The critical values (D<sub>c</sub>) of the KS statistic are also shown. In all cases, D < D<sub>c</sub> indicating that there is no significant difference between the distributions. In addition to the populations (i) – (iii), we also considered another set (i) + (iii) consisting of SC 25 SGREs and LAT-gap DH type II bursts. The HXR durations in this set is similar to the other ones as confirmed by the KS test.

**Table 3.** Comparison of various duration distributions

Duration Comparison	N1, N2	D	D <sub>c</sub>
SC25 vs. SC 24	10, 25	0.3000	0.5149
DHgap vs. SC 24	27, 25	0.2533	0.3819
DHgap + SC 25 vs. SC 24	37, 25	0.1632	0.3562
DHgap + SC25 vs. SC 24 All	37, 31	0.1787	0.3350

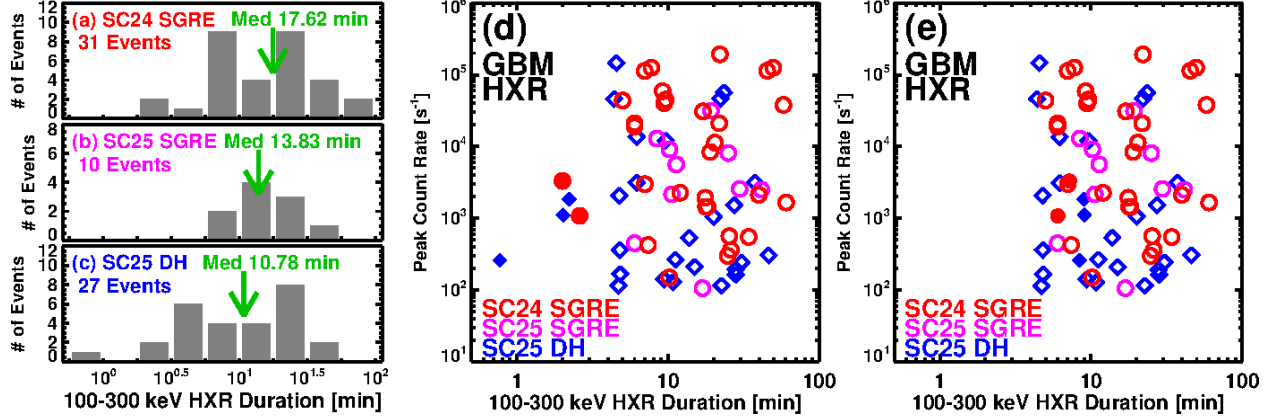


**Figure 4.** Distributions of >100 keV HXR bursts associated with (a) SC 24 SGREs, (b) SC 25 SGREs, and (c) SC 25 DH type II bursts that occurred during the LAT data gaps. (d) Scatter plot of the >100 keV HXR bursts vs. their peak count rate for the three populations shown in (a-c). The number of events (N) in each population is shown on the plots. The leftmost 5 events that have HXR durations < 2.6 min are indicated by filled symbols. The durations of these events are severely underestimated due to the 100 counts/s threshold. (e) Same as (d) but after correcting the durations of the filled symbol events in (d).

The good overlap of >100 keV HXR durations among DH type II bursts and SGRE events in the two cycles is illustrated in Fig. 4d as a scatter plot between the 100-300 keV HXR duration and the peak count rate. The overlap is consistent with the close relation between the two phenomena.

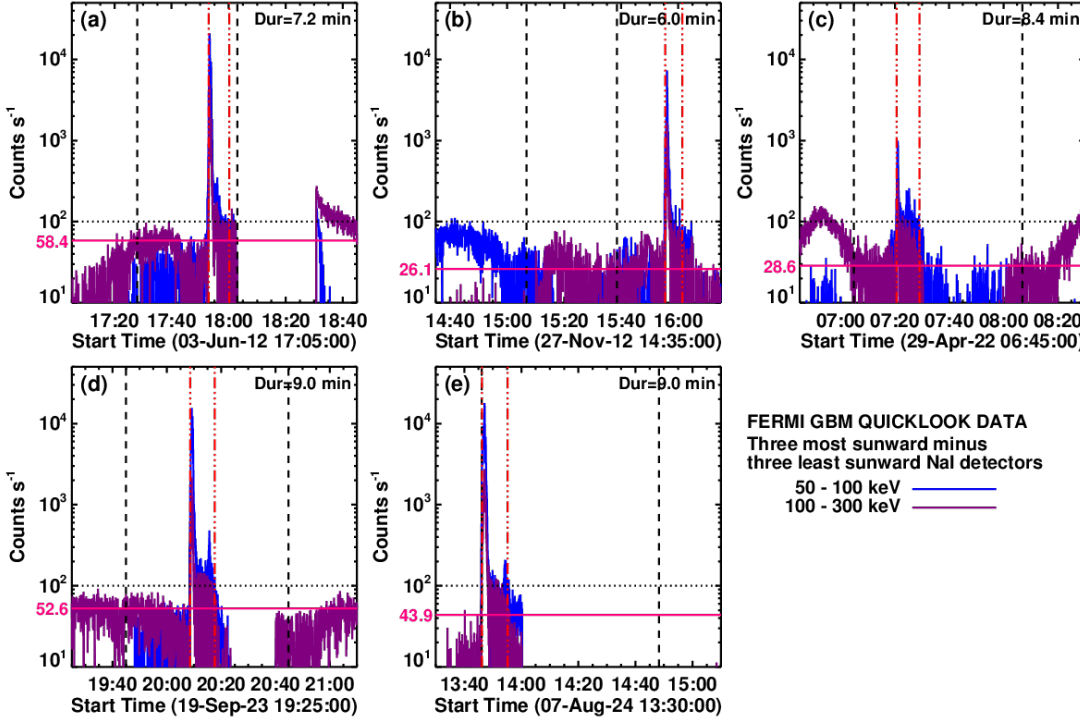


**Figure 5.** Fermi/GBM light curves in the energy channels 50-100 keV (blue) and 100-300 keV (purple) of 5 HXR bursts that showed the shortest  $>100$  keV durations. The 2012 June 3 and 2012 November 27 are associated with SC 24 SGREs. The other three are associated with DH type II bursts that occurred during the Fermi/LAT data gap. In all events there is a second HXR peak (prominent in the 50-100 keV channel) within the impulsive phase. The dotted horizontal line at 100 counts/s was originally used to estimate the duration. The actual background is smaller than 100 counts/s by a factor of  $\sim 2\text{-}4$ , and is shown by the horizontal red line. The background was determined based on the average counts over 5 minutes before the starting point and after the ending point above 100 counts/s. The greater of the two is used as the background and is given on the plots. The HXR duration is marked by the pair of red dot-dashed vertical lines in each plot. The vertical black dashed lines denote Fermi's day-night boundaries.

There are five HXR bursts of duration in the range 0.77 to 2.60 min shown by filled symbols at the left end of the plot in Fig. 4d. Two of them are SC 24 SGRE events (Table 3) and three are LAT-gap DH type II bursts (Table 4). A closer look at the GBM light curves indicates that the background HXR level in these events is much lower than the 100 counts/s that we used as the threshold for measuring the duration. When the actual background is used, the durations of these five events are significantly longer. Figure 8 shows the light curves of these events indicating that their estimated durations range from 6 min to 9 min, on par with the other HXR events in Tables 2-4. The scatter plot in Fig. 4e uses the corrected durations for these 5 events. Using the actual background allows the inclusion of secondary HXR peaks in the impulsive phase as can be seen in Fig. 5. These considerations suggest that the association of  $>100$  keV HXR bursts of

long duration ( $>\sim 5$  min) along with DH type II bursts is a necessary condition for the production of SGRE. This result is consistent with the fact that only long-duration  $>100$  keV HXR bursts are associated with CMEs, while the impulsive short duration ones are not associated with CMEs (Mäkelä et al. 2025, in this topical issue). These authors investigated all the  $>100$  keV GBM HXR bursts that occurred after the SADA anomaly (2018-2024). A total of  $\sim 200$  bursts were identified including those in Tables 2 and 4. Only 137 of the 200 HXR are associated with CMEs. When not associated with a CME, the HXR durations are much smaller, typically  $<1$  min.

### 3.5 Estimating the Number of SGRE Events in SC 25

The above discussion showed that SGRE events and the 27 LAT-gap DH type II bursts have similar characteristics in terms CME speeds, flare sizes, and particularly  $>100$  keV HXR durations. Therefore, we suggest that the 27 LAT-gap type II bursts must be indicative of SGRE. Adding these 27 to the 15 SGRE events that were actually observed by Fermi/LAT brings the total number to 42 in SC 25. A second way is to assume that the number of SGRE events follows SSN: the average SSN increased from 56.9 in SC 24 to 79.0 in SC 25, or by 39%, so the number in SC 25 should be  $\sim 35$  ( $25 \times 1.39$ ). However, the number of FW CMEs and DH type II bursts increased more than SSN did by 29% and 33%, respectively. Therefore, the SSN-based estimate (35) needs to be boosted by 29% and 33%, respectively to yield 45 and 47 SGRE events in SC 25. A third way is to use the observation that 17% of all FW CMEs and 25% of all DH type II bursts produced SGRE events in SC 24 (see Table 1). If these association rates hold good in SC 25, we expect  $\sim 46$  SGRE events (17% of 268 FW CMEs or 25% of 183 DH type II bursts). This number is the same as that from SSN-based and is only about 9.5% higher than that estimated based on HXR burst association. The average value from the three methods is 45 SGRE events. Given the variation in the heliospheric properties that modulate the shock strength, we think that the estimated number of SGRE events in SC 25 is reasonable and consistent among different methods.

## 4. Discussion

One of the detailed investigations we made is the long duration ( $>\sim 5$  min) of  $>100$  keV HXR bursts associated with SGRE events. Many studies have shown that gradual HXR (GHX) bursts are closely associated with large SEP events (Kiplinger 1995; Garcia 1994). GHX typically have durations  $> 10$  min as opposed to impulsive HXR (IHX) bursts that have a duration  $<2$  min. The long duration GBM HXR bursts clearly belong to the GHX bursts from the past. One of the main characteristics of GHX bursts is that the associated flares have a lower temperature, which is proportional to the soft X-ray flux ratio  $R$  (0.04-0.5 nm to 0.1-0.8 nm). Ling and Kahler (2020) and Kahler and Ling (2020) have shown that  $R$  is also a good indicator of FW CMEs. Large SEP events and DH type II bursts are also associated with FW CMEs because these CMEs drive

shocks that accelerate electrons and protons (Gopalswamy et al. 2001; 2004). Thus, we see that the GHX link to SEPs and FW CMEs extends to DH type II bursts, which we utilized in this paper. Another key characteristic of GHX bursts is their soft-hard-harder spectral profile (Kiplinger 1995). As noted by Share et al. (2018),  $>100$  keV HXR bursts have a harder spectrum than the ones at lower energies ( $<50$  keV). We see that all phenomena associated with energetic CMEs (large SEP events, DH type II bursts, and shocks) are accompanied by  $>100$  keV HXR bursts. Although there is no definite answer for the observed connection between  $>100$  keV HXR and FW CMEs, they are inevitably tied together by the same magnetic reconnection. While both DH type II bursts and SEPs are definitely CME related (via shock), SEPs have an additional potential source - flare reconnection. Complex type III bursts that invariably accompany large eruptions are indicative of open magnetic field lines along which electrons accelerated from the flare site escape into the interplanetary medium (Cane, Erickson, & Prestage 2002, Gopalswamy et al. 2012, Winter and Ledbetter, 2015; Gopalswamy et al. 2023b). This escape channel should be available for flare ions as well that may be reaccelerated by the accompanying CME-driven shock (Share et al. 2018).

The 2011 June 2 event did not have GBM observations, but the underlying CME was fast and ( $976$  km s $^{-1}$ ) wide (halo CME) with an associated DH type II burst. Share et al. (2018) investigated this event and pointed out that the flare was observed by the Reuven Ramaty High-Energy Solar Spectroscopic Imager (RHESSI, Lin et al. 2002) in hard X-rays only for the first three minutes (07:33 UT to 07:36 UT). So, we cannot say whether the HXR emission was long duration or not. Furthermore, this event had a special situation in that there were two CMEs launched from the same active region separated by only  $\sim 1$  hr. The associated flares were weak with soft X-ray class of C1.4 and C3.7. Figure 6 shows two prominence eruptions (P1, P2) associated with the two soft X-ray flares (F1 and F2) and homologous EUV waves (Waves 1 and Waves 2). In the SOHO/LASCO catalog, the first eruption had a slow ( $253$  km s $^{-1}$ ) but wide ( $61^\circ$ ) CME appearing at 07:24 UT. The second CME was a fast ( $976$  km s $^{-1}$ ) halo with a first-appearance time of 08:12 UT. Given the disk-center location of the source active region (AR 11227), these sky-plane speeds are expected to be much smaller than the true speeds. The STEREO-Behind spacecraft was located at E93 at the time of the eruptions, so the two CMEs were observed as limb events in its FOV (at W73 and W78). The first appearance time and height of the of the CMEs are 06:45:34 UT at 1.73 Rs (CME 1) and 07:45:35 UT at 2.34 Rs (CME 2). Tracking the leading edges, we found that both CMEs were accelerating in the COR1 FOV and had a speed of  $818$  km s $^{-1}$  (CME 1) and  $1237$  km s $^{-1}$  (CME 2) by the time they reached the edge of the FOV around 4 Rs. Gopalswamy et al. (2019a) suggested that the first CME might have provided a mirroring situation, so that the protons accelerated by the second CME were directed sunward to precipitate and produce SGRE.

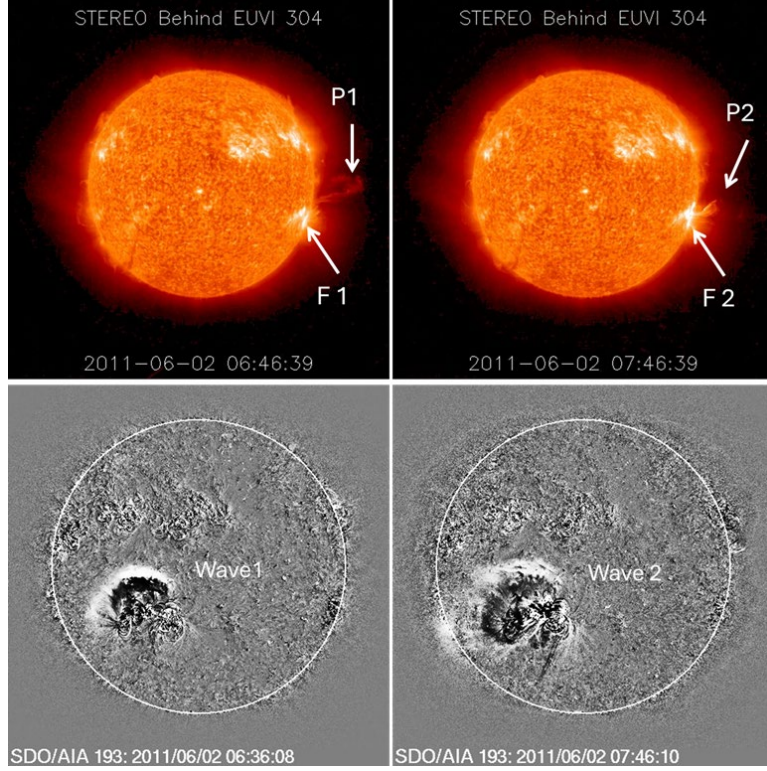


**Figure 6.** Two eruptions from NOAA active region 11227 that occurred during 2011 June 2. (top) prominence eruptions (P1 and P2) flares (F1 and F2) associated with the event in STEREO-Behind EUV images at 304 Å taken at 06:46 UT and 07:46 UT. In soft X-rays (GOES), F1 was a C1.4 flare from S19E20 (06:30 UT) while F2 was a C3.7 flare from S19E25 (07:22 UT). (bottom) homologous EUV disturbance (Wave 1 and Wave 2) revealed by the 193 Å running difference images at 06:36 UT and 07:46 UT from the Atmospheric Imaging Assembly (Lemen et al. 2012) on board the Solar Dynamics Observatory (SDO/AIA).

## 5. Summary

Studies of Fermi/LAT observations have shown that there is a close relation among SGRE events, FW CMEs, large SEP events, and interplanetary type II bursts. The reason behind this relation is as follows: the FW CMEs drive strong shocks that accelerate protons responsible for SGRE events and SEP events, while the accelerated electrons result in type II radio bursts. The energetic ions responsible for SGRE are thought to propagate from the shock toward the Sun while those propagating away into space are detected as SEP events. Previous studies have shown that the solar cycle variation of the occurrence rates of SEP events and IP type II bursts generally follow that of the FW CMEs. Since SGRE events are associated with these energetic phenomena, we expected their occurrence rate to have a similar behavior. However, we observed a reduction in the number of SGRE events in SC 25 relative to the weaker SC 24. The reduction seems to be primarily due to Fermi/LAT's reduced Sun exposure following the malfunction of

the solar array drive assembly since March 16, 2018. Invoking the close connection between >100 keV hard X-ray bursts and SGRE events, we identified such bursts during Fermi/LAT data gaps. When such hard X-ray bursts are also associated with DH type II bursts in the gaps, we suggest that such combination is indicative of an SGRE event. By this method, we estimated that the total number of SGRE events in SC 25 is ~42, which is consistent with what is expected (~46) from the fraction of FW CMEs and DH type II bursts associated with SGRE events in SC 24. The estimated number of SGRE events is consistent with the fact that SC 25 is stronger than SC 24. The primary conclusions of this work are as follows.

1. The halo CME abundance in SC 25 is lower than that in SC 24 consistent with the previous studies which showed that weaker solar cycles have higher halo abundance.
2. Although the number of large SEP events was higher in SC 25, the increase was not commensurate with solar activity (SSN). The change in the ambient magnetosonic speed and the magnetic connectivity might have affected the SEP event number.
3. The number of fast and wide CMEs and DH type II bursts increased in SC 25 more than SSN did by 29% and 33%, respectively.
4. The ratio of FW CME to DH type II numbers remains the same between SCs 24 (66%) and 25 (68%) confirming their physical connection (fast and wide CMEs drive shocks that accelerate electrons to produce type II bursts).
5. Only a small fraction of fast and wide CMEs (17%) and DH type II bursts (25%) are associated with SGRE events in SC 24.
6. Hard X-ray bursts at energies >100 keV when accompanied by DH type II bursts are good indicators of SGRE events evidenced by the observations in SCs 24 and 25.
7. Hard X-ray bursts at energies >100 keV have a long duration ( $>\sim 5$  min) when accompanying fast and wide CMEs, DH type II bursts, and large SEP events.
8. Based on the association with >100 keV HXR bursts, we estimate that 27 DH type II bursts that occurred during the Fermi/LAT data gaps are likely to be SGRE events: thus, bringing the total number of SGRE events in SC 25 to 42.
9. The number of SC 25 SGRE events estimated from the SC 24 association rate between FW CMEs and DH type II bursts is ~45 and 47, respectively, not too different from the estimate based on >100 keV HXR bursts.
10. If the number of SGRE events followed SSN, we should have 35 SGRE events in SC 25. However, if the overabundance of FW CMEs and DH type II bursts relative to SSN applies to SGRE, we get 45 and 46 SGRE events, respectively.
11. The estimated number of SGRE events in SC 25 is consistent with the observation that SC 25 is stronger than SC 24.
12. Energetic phenomena such as fast and wide CMEs, halo CMEs, DH type II bursts, GLE events, and intense geomagnetic storms all indicate a stronger SC 25, consistent with the estimated number of SC 25 SGRE events.

## Funding

NG is supported by Goddard Space Flight Center, LWS-HSSO, STEREO Project, and NASA Science Mission Directorate, 2024 HISFM. SY, PM, HX, SA are partially supported by Goddard Space Flight Center, PHaSER-670.089. SA and HX are also supported by US National Science Foundation, AGS-2228967.

## Acknowledgments

The Fermi mission is a joint venture of NASA, the United States Department of Energy, and government agencies in France, Germany, Italy, Japan, and Sweden. We acknowledge the use of the Fermi Solar Flare Observations facility funded by the Fermi GI program ([https://hesperia.gsfc.nasa.gov/fermi\\_solar/](https://hesperia.gsfc.nasa.gov/fermi_solar/)). Wind-Konus flare data are from <https://www.ioffe.ru/LEA/sun.html>. The Global Geospace Science (GGS) Wind is a NASA science spacecraft designed to study radio waves and plasma that occur in the solar wind and in the Earth's magnetosphere. SDO is part of NASA's LWS program. SOHO is a project of international collaboration between ESA and NASA. STEREO is the third mission in NASA's Solar Terrestrial Probes (STP) program. Geostationary Operational Environmental Satellites (GOES) is a collaborative NOAA and NASA program providing continuous imagery and data. We thank Elizabeth Hays, Fermi Project Scientist, for discussion on the 2018 solar array drive anomaly.

## References

Ajello, M., Baldini, L., Bastieri, D., et al.: 2021, First Fermi-LAT Solar Flare Catalog. *Astrophys. J. Sup.*, 252, 13.

Allafort, A. J.: 2018, High-energy gamma-ray observations of solar flares with the Fermi large area telescope. PhD thesis, Stanford Univ.

Aptekar R. L., Frederiks D. D., Golenetskii S. V., Ilynskii, V. N., Mazets, E. P., Panov, V. N. et al. 1995, Konus-W Gamma-Ray Burst Experiment for the GGS Wind Spacecraft, *SSRv* 71 265

Atwood, W. B., Abdo, A. A., Ackermann, M., et al.: 2009, The Large Area Telescope on the Fermi Gamma-Ray Space Telescope Mission. *Astrophys. J.*, 697, 1071.

Bougeret, J.-L., Kaiser, M. L., and Kellogg, P. J.: 1995, Waves: The Radio and Plasma Wave Investigation on the Wind Spacecraft. *Space Sci. Rev.*, 71 231.

Bougeret, J.-L. Goetz, k., Kaiser, M. L., et al.: 2008, S/WAVES: The Radio and Plasma Wave Investigation on the STEREO Mission. *Space Sci. Rev.*, 136, 487. doi : 10.1007/s11214-007-9298-8

Brueckner, G. E., Howard, R. A., Koomen, M. J. et al.: 1995, The Large Angle Spectroscopic Coronagraph (LASCO). *Solar Phys.*, 162, 357.

Cane, H. V., Erickson, W. C., Prestage, N. P.: 2002, Solar flares, type III radio bursts, coronal mass ejections, and energetic particles. *J. Geophys. Res.*, 107, Issue A10, CiteID 1315, doi: 10.1029/2001JA000320

Forrest, D. J., Vestrand, W. T., Chupp, E. L., et al.: 1985, Neutral Pion Production in Solar Flares. *Proc. of 19th International Cosmic Ray Conf. (ICRC19)*, 4, 146.

Garcia, H. A.: 1994, Temperature and Hard X-Ray Signatures for Energetic Proton Events. *Astrophys. J.*, 420, 422. doi:10.1086/173572

Gopalswamy, N.: 2018, Extreme Solar Eruptions and their Space Weather Consequences. Extreme Events in Geospace. Origins, Predictability, and Consequences, Edited by Natalia Buzulukova. ISBN: 978-0-12-812700-1. Elsevier, p.37-63

Gopalswamy, N., Yashiro, S., Kaiser, M. L., Howard, R. A., Bougeret, J.-L.: 2001, *J. Geophys. Res.*, 106, Issue A12, 29219. doi:10.1029/2001JA000234

Gopalswamy, N., Yashiro, S., Krucker, S., Stenborg, G., Howard, R. A.: 2004, Intensity variation of large solar energetic particle events associated with coronal mass ejections. *J. Geophys. Res.*, 109, Issue A12, CiteID A12105. doi:10.1029/2004JA010602

Gopalswamy, N., Yashiro, S., Michalek, G., Stenborg, G., Vourlidas, A., Freeland, S., Howard, R. A.: 2009, The SOHO/LASCO CME catalog, *Earth, Moon, and Planets*, 104, 295. <https://doi.org/10.1007/s11038-008-9282-7>.

Gopalswamy, N., Yashiro, S., Michalek, G., et al.: 2010, A Catalog of Halo Coronal Mass Ejections from SOHO. *Sun and Geosphere*, 5, 7.

Gopalswamy, N., Xie, H., Yashiro, S., Akiyama, S., Mäkelä, P., Usoskin, I. G.: 2012, Properties of Ground Level Enhancement Events and the Associated Solar Eruptions During Solar Cycle 23. Doi: 10.1007/s11214-012-9890-4

Gopalswamy, N., Xie, H., Akiyama, S., Yashiro, S., Usoskin, I. G., Davila, J. M.: 2013, The First Ground Level Enhancement Event of Solar Cycle 24: Direct Observation of Shock Formation and Particle Release Heights. *Astrophys. J. Lett.*, 765, L30. Doi: 10.1088/2041-8205/765/2/L30

Gopalswamy N, Mäkelä P: 2014, Latitudinal connectivity of ground level enhancement events. *ASP Conference Series*, vol 484. In Outstanding problems in heliophysics: from coronal heating to the edge of the heliosphere Edited by: Hu Q, Zank G., p. 63.

Gopalswamy, N., Akiyama, S., Yashiro, S.: 2014, Anomalous expansion of coronal mass ejections during solar cycle 24 and its space weather implications. *Geophys. Res. Lett.*, 41, 2673, <https://doi.org/10.1002/2014GL059858>.

Gopalswamy, N., Yashiro, S., Xie, H., Akiyama, S., Mäkelä, P.: 2015a, Properties and geoeffectiveness of magnetic clouds during solar cycles 23 and 24. *J. Geophys. Res.*, 120, 9221. <https://doi.org/10.1002/2015JA021446>

Gopalswamy, N., Xie, H., Akiyama, S., Mäkelä, P., Yashiro, S., Michalek, G.: 2015b, The Peculiar Behavior of Halo Coronal Mass Ejections in Solar Cycle 24. *Astrophys. J.*, 804, L23. Doi: 10.1088/2041-8205/804/1/L23

Gopalswamy, N., Mäkelä, P., Yashiro, S., et al.: 2018, Interplanetary Type II Radio Bursts from Wind/WAVES and Sustained Gamma-Ray Emission from Fermi/LAT: Evidence for Shock Source. *Astrophys. J. Lett.*, 868, L19.

Gopalswamy, N., Mäkelä, P., Yashiro, S., et al.: 2019a, On the Shock Source of Sustained Gamma-Ray Emission from the Sun. *J. Phys. Conf. Series*, 1332, 012004.

Gopalswamy, N., Mäkelä, P., Yashiro, S.: 2019b, A Catalog of Type II radio bursts observed by Wind/WAVES and their Statistical Properties. *SunGeo*, 14, 111

Gopalswamy, N., Yashiro, S., Mäkelä, P., et al.: 2021, The Common Origin of High-energy Protons in Solar Energetic Particle Events and Sustained Gamma-Ray Emission from the Sun. *Astrophys. J.*, 915, 82, doi : 10.3847/1538-4357/ac004f

Gopalswamy, N., Mäkelä, P., Yashiro, S., Akiyama, S., Xie, H.: 2022, Solar activity and space weather. *J. Phys. Conf. Ser.*, Vol. 2214, Issue 1, id.012021. doi:10.1088/1742-6596/2214/1/012021

Gopalswamy, N., Michalek, G., Yashiro, S., Akiyama, S., Hong, X: 2023a, What Do Halo CMEs Tell Us about Solar Cycle 25? *Astrophys. J. Lett.*, 952, L13

Gopalswamy, N., Kumari, A., Makela, P.: 2023b, Type III Radio Bursts from Solar Eruptions and their Connection to GLE and SGRE Events. 2023 XXXVth General Assembly and Scientific Symposium of the International Union of Radio Science (URSI GASS), Sapporo, Japan, 2023, pp. 1-3, doi: 10.23919/URSIGASS57860.2023.10265368

Gopalswamy, N., Michalek, G., Yashiro, S., Mäkelä, P., Akiyama, S., Xie, Hong; Vourlidas, A.: 2024, The SOHO LASCO CME Catalog -- Version 2. *Proc. IAU Symposium* 388, doi:10.48550/arXiv.2407.04165

Gopalswamy N., Mäkelä P. A., Akiyama S., Yashiro S., Xie H.: 2025a, Solar Cycle Variation of Sustained Gamma-ray Emission Events from the Sun and Related Energetic Events. *Proceedings of the Seventeenth Workshop on Solar Influences on the Magnetosphere, Ionosphere and Atmosphere*, pp. 24–33. <https://doi.org/10.31401/WS.2025.proc.04>

Gopalswamy, N., Mäkelä, P., Akiyama, S., et al.: 2025b, Multispacecraft observations of the 2024 September 9 backside solar eruption that resulted in a sustained gamma-ray emission event, *Solar Phys.*, 300, 120, <https://doi.org/10.1007/s11207-025-02526-9>.

Howard, R. A., Michels, D. J., Sheeley, N. R. Jr., Koomen, M. J.: 1982, The Observation of a Coronal Transient Directed at Earth. *Astrophys. J.*, 263, L101.

Howard, R. A., Sheeley, N. R. Jr., Michels, D. J., Koomen, M. J.: 1985, Coronal Mass Ejections: 1979– 1981. *J. Geophys. Res.*, 90, 8173

Howard, R. A., Moses, J. D., Vourlidas, A., et al.: 2008, Sun Earth Connection Coronal and Heliospheric Investigation (SECCHI), *Space Sci. Rev.*, 136, 67.

Kahler, S. W., Ling, A. G.: 2020, The Role of Peak Temperatures in Solar X-Ray Flare Associations with CME Speeds and Widths and in Flare Size Distributions. *Astrophys. J.*, 901, 63. doi:10.3847/1538-4357/abae5e

Kanbach, G., Bertsch, D. L., Fichtel, C. E., et al.: 1993, Detection of a long-duration solar gamma-ray flare on June 11, 1991 with EGRET on COMPTON-GRO. *Astr. Astrophys. Sup.*, 97, 349.

Kiplinger, A. L.: 1995, Comparative Studies of Hard X-Ray Spectral Evolution in Solar Flares with High-Energy Proton Events Observed at Earth. *Astrophys. J.*, 453, 973. doi: 10.1086/176457

Kirkman, T. W.: 1996, Statistics to Use. <http://www.physics.csbsju.edu/stats/> (16 November 2025).

Krucker, S., Hurford, G. J., Grimm, O., et al.: 2020, The Spectrometer/Telescope for Imaging X-rays (STIX). *Astr. Astrophys.*, 642, A15.

Lemen, J. R., Title, A. M., Akin, D. J., et al.: 2012, The Atmospheric Imaging Assembly (AIA) on the Solar Dynamics Observatory (SDO). *Solar Phys.*, 275, 17.

Lin, R. P., Dennis, B. R., Hurford, G. J. et al. : 2002, The Reuven Ramaty High-Energy Solar Spectroscopic Imager (RHESSI). *Solar Phys.* 210, 3

Ling, A. G., Kahler, S. W.: 2020, Peak Temperatures of Large Solar X-Ray Flares and Associated CME Speeds and Widths. *Astrophys. J.*, 891, 54. doi:10.3847/1538-4357/ab6f6c

Lysenko, A. L., Ulanov, M. V., Kuznetsov, A. A. et al.: 2022, KW-Sun: The Konus-Wind Solar Flare Database in Hard X-Ray and Soft Gamma-Ray Ranges, *Astrophys. J. Suppl. Ser.*, 262, 32. doi: 10.3847/1538-4365/ac8b87

Meegan, C., Lichti, G., Bhat, P. N., Bissaldi, E., Briggs, M. S., Connaughton, V. et al. (2009), The Fermi Gamma-ray Burst Monitor. *Astrophys. J.*, 702, 791

Nandy, D.: 2021, Progress in Solar Cycle Predictions: Sunspot Cycles 24-25 in Perspective. *Solar Phys.*, 296, 54. doi:10.1007/s11207-021-01797-2

Pesce-Rollins, M., Omodei, N., Krucker, S., et al.: 2022, The Coupling of an EUV Coronal Wave and Ion Acceleration in a Fermi-LAT Behind-the-Limb Solar Flare. *Astrophys. J.*, 929, 172.

Share, G. H., Murphy, R. J., Tolbert, A. K., et al.: 2018, Characteristics of Late-phase  $>100$  MeV Gamma-Ray Emission in Solar Eruptive Events. *Astrophys. J.*, 869, 182.

Thompson, D. T., Wilson-Hodge, C. A.: 2022, Fermi Gamma-ray Space Telescope, <https://doi.org/10.48550/arXiv.2210.12875>

Winter, L. M., Ledbetter, K.: 2015, Type II and type III radio bursts and their correlation with Solar energetic proton events. *Astrophys. J.*, 809, 105. <http://dx.doi.org/10.1088/0004-637X/809/1/105>

Yashiro, S., Gopalswamy, N., Akiyama, S., et al.: 2024, Estimation of Soft X-ray Fluxes of Behind-the-Limb Flares Using STEREO EUV Observations. American Geophysical Union Fall Meeting, Abstract # SH23D-2972.